Optics and Laser Technology 98 (2018) 169–177

Contents lists available at ScienceDirect

Optics and Laser Technology

journal homepage: www.elsevier.com/locate/optlastec

Full length article

Tunable few-cycle pulses from a dual-chirped optical parametric amplifier pumped by broadband laser

Zuofei Hong [a], Qingbin Zhang [b,*], S. Ali Rezvani [b], Pengfei Lan [b], Peixiang Lu [a,b]

[a] Laboratory of Optical Information Technology, Wuhan Institute of Technology, Wuhan 430205, China
[b] School of Physics and Wuhan National Laboratory for Optoelectronics, Huazhong University of Science and Technology, Wuhan 430074, China

ARTICLE INFO

Article history:
Received 7 December 2016
Received in revised form 24 July 2017
Accepted 26 July 2017
Available online 12 August 2017

Keywords:
Broadband laser
Dual-chirped OPA
Few-cycle pulses

ABSTRACT

We propose a dual-chirped optical parametric amplification (DC-OPA) scheme pumped by a broadband laser pulse. The pump pulse is spectrally broadened in a multi-plate system before amplifying the chirped seed in a BBO crystal. The system performance and phase-matching mechanism with different pump bandwidths are investigated thoroughly. It is found that the broadened pump bandwidth benefits the system most effectively when the pump and seed pulses are oppositely chirped. The idler bandwidth is nearly tripled in the broadband pumped system, supporting a transform-limited (TL) duration of 8.4 fs (~1.3 cycles), meanwhile the energy bandwidth product of the idler is 72.6% higher. Furthermore, the idler wavelength is tunable between 1700 nm and 2050 nm, with sub-1.5-cycle TL duration and over 14% conversion efficiency. The proposed scheme provides a suitable approach for the generation of few-cycle pulses varying from near-infrared to mid-infrared regions.

1. Introduction

Few-cycle laser pulses with microjoule to millijoule energy have attracted lots of attentions in the past decades, owing to their utmost importance for applications including strong-field physics, attosecond optics, and ultrafast spectroscopy [1–11]. The special properties of titanium doped sapphire (Ti:sapphire) such as broadband lasing range from 600 to 1050 nm, high stability, and indefinitely long lifetime, make it a suitable material for a femtosecond laser [12,13]. Using Kerr lens mode-locking (KLM) technique accompanied with chirped pulse amplification (CPA) [14], Ti:sapphire laser has become one of the most popular commercially-available sources for energetic ultrashort laser pulses. However, the CPA technology is not capable of producing high-energy femtosecond pulses in >1 μm range, due to the lack of suitable laser material. Optical parametric amplification (OPA) and optical parametric chirped pulse amplification (OPCPA), with their outstanding advantages including broad gain bandwidth, high wavelength tunability, lower accumulation of thermal load and undesired nonlinear effects, have become promising methods to down-convert the Ti:sapphire laser light [15–18].

An ultra-broadband gain is essential for few-cycle pulse generation in OPA. The zero group velocity mismatch (GVM) at degeneracy allows ultrabroad gain bandwidth and few-cycle duration of the output pulses, but the central wavelength is strictly limited with low tunability [19–22]. For non-degenerate signal and idler pulses, the increasing GVM leads to a much narrower gain bandwidth. By using non-collinear geometry, the group velocity (GV) of signal equals the projection of idler GV along the propagation direction, the amplified pulses can therefore be overlapped over a long interacting distance, producing a signal pulse with larger bandwidth [23–27]. Nevertheless, the non-collinear pump-seed angle will result in an idler beam with angular dispersion, which requires energy-consuming dispersion compensation stage for its further use [28,29].

In order to produce few-cycle pulses at non-degenerate wavelength in a collinear OPA, several approaches have been proposed. For example, employing periodically poled crystals to obtain broadband gain in a quasi-phase-matched (QPM) OPA [30–32], broadening the spectral bandwidth of OPA output pulse with a hollow fiber [33,34], or amplifying the pulse in the frequency domain (Frequency-domain OPA, FOPA) [35,36], etc. However, the aperture and damage threshold of periodically poled crystals as well as the hollow core fiber severely limit the available pulse energy, and the FOPA requires complex management of the interacting pulses spatially and temporally.

* Corresponding author.
E-mail address: zhangqingbin@hust.edu.cn (Q. Zhang).

http://dx.doi.org/10.1016/j.optlastec.2017.07.042
0030-3992/

A comparatively simpler method to enhance the energy scalability is the dual-chirped OPA (DC-OPA) scheme [37–40]. Zhang et al. proposed DC-OPA scheme in [37]. The authors chirped both pump and seed pulses to decrease the peak intensity of interacting pulses and prevent undesired nonlinear effects. It was found that the DC-OPA scheme is potentially capable of generating IR pulses with the energy of few hundred millijoule. Fu et al. implemented DC-OPA with a 100-mJ pump laser and obtained 20-mJ uncompressed signal at 1400 nm, a total conversion efficiency over 30% is experimentally achieved [38]. Wandel et al. extended the DC-OPA scheme to longer wavelengths and generated narrowband, high-energy, bandwidth-tunable pulses in the mid-infrared (mid-IR) region [40]. Even though the DC-OPA scheme shows excellent energy scalability, the signal or idler bandwidths are not broad enough to support few-cycle output pulses for many important applications, e.g. generation of isolated attosecond pulse (IAP) in extreme ultraviolet range [41,42].

The gain bandwidth in DC-OPA can be increased by introducing the concept of chirp-compensation [43–46]. The time-dependent instantaneous wavelengths of pump and seed pulses are carefully tailored in a way that ensures perfect phase-matching for a wide range of frequency components, thus broadband gain is obtained. Tang et al. implemented a chirp-compensation OPCPA scheme and amplified a spectrum with more than 165-nm bandwidth and less than 15-fs TL duration [43]. In [44], Limpert et al. utilized the chirp compensation scheme for a degenerate signal, with the second harmonic of a Ti:sapphire laser as the pump, the generated signal spectrum covers a range of 630–1030 nm. Similarly, we proposed the dual-pump OPCPA scheme [47] in which two non-degenerate regions of the chirped seed are amplified by two chirped pump respectively, the output spectrum spanning from 1300 nm to 2100 nm is obtained with a TL pulse duration of 9.0 fs. Recently, Yin et al. presented a broadband-pumped DC-OPA system for the generation of high-energy, two-cycle pulses centered at 3.2 μm [48].

According to our study on the dual-pump OPCPA scheme, the gain bandwidth of the system can benefit from a broader pump bandwidth [47]. However, most of the existing OPAs utilized the pump pulse directly from a laser system with a TL duration of >30 fs. Energetic 800-nm pulses with broader bandwidth and shorter TL duration are readily available with current technique. Lu et al. generated an intense super-continuum by focusing a high-power laser pulse into several pieces of strategically placed fused silica plates [49]. In [50], He et al. also performed the multi-plate scheme and achieved 800-nm, 0.68-mJ, 5.4-fs pulse with a near-single-cycle TL duration of 3.5-fs. It is naturally inferred that if the high-energy, broadband pulses are utilized to pump an OPA, the gain bandwidth of the system can be remarkably improved.

In this paper, we propose a DC-OPA system pumped by a broadband femtosecond laser. Instead of pumping the system directly from a Ti:sapphire laser source, the pulse is sent into a multi-plate system for spectral broadening. The broadband pump and seed pulses are both chirped to manipulate their time-dependent wavelengths and improve the gain efficiency. The amplification mechanism at different pump bandwidths and chirp combinations is investigated and discussed, and the system performance is optimized correspondingly. The spectral-temporal property of the idler pulse from a broadband pump OPA is specifically analyzed and the wavelength tunability is confirmed. The rest of this paper is arranged as follows. In Section 2, we introduce the concept and numerical model of the proposed scheme. In Section 3, the gain mechanism of DC-OPA is analyzed. In Section 4, the results of broadband pumped and narrowband pumped DC-OPAs are compared. Finally in Section 5, the conclusions are drawn and the prospect is discussed.

2. Concept and theory

The schematic of the proposed scheme is presented in Fig. 1. The initial pulse is produced in a commercially available Ti:sapphire laser with a pulse duration of 50 fs and a repetition rate of 1 kHz. The laser beam is divided into two beams. The beam with higher pulse energy is spectrally broadened in a multi-plate system, and then temporally chirped in the pump stretcher. The less energetic beam passes through a dual-crystal OPA (DOPA) system to produce a broadband seed centered at 1400 nm [51,52]. The seed pulse is chirped in a seed stretcher. In order to compare different systems with different pump bandwidths, we simulate the amplification process using Gaussian-shaped pump pulses with TL durations of 10 fs, 20 fs, 30 fs, and 50 fs, respectively. The shorter the TL duration is, the broader the pump bandwidth is. The pulse energy is fixed at 300 μJ. For simplicity and clarity in the following article, the 50-fs pump pulse will be referred to as the narrowband pump (although the bandwidth is considerably large), in comparison to the broadband pump with 10-fs to 30-fs TL duration. It is noteworthy that, since all existing bandwidth-broadening methods inevitably stretch the pulse temporally and the recompression requires deliberate dispersion management, the broadband pumps will not be used as TL pulses here. Instead, each broadband pump pulse is chirped and stretched to a designed pulse duration, varying from 50 fs to 120 fs. The seed spectrum is obtained from our recent experiment [52], with a full width at half maximum (FWHM) bandwidth over 200 nm. The TL duration of the seed is 13 fs and the pulse energy is approximately 1 μJ. Both the radii of the pump and seed beams are 5 mm.

To quantitatively investigate the influence of pump bandwidth on OPA system, we numerically solve the coupled wave equations including the nonlinear interaction and up to fourth order dispersion of each pulse, which are written as follows:

$$\frac{\partial}{\partial z}A_p + \sum_{j=2}^{n}\frac{(-i)^{j-1}}{j!}k_p^{(j)}\frac{\partial^j}{\partial\tau^j}A_p = \frac{id_{eff}\omega_p}{n_p c}A_s A_i e^{i\Delta kz},$$

$$\frac{\partial}{\partial z}A_s + \left(\frac{1}{v_{gs}}-\frac{1}{v_{gp}}\right)\frac{\partial}{\partial\tau}A_s + \sum_{j=2}^{n}\frac{(-i)^{j-1}}{j!}k_s^{(j)}\frac{\partial^j}{\partial\tau^j}A_s = \frac{id_{eff}\omega_s}{n_s c}A_p A_i^* e^{-i\Delta kz},$$

$$\frac{\partial}{\partial z}A_i + \left(\frac{1}{v_{gi}}-\frac{1}{v_{gp}}\right)\frac{\partial}{\partial\tau}A_i + \sum_{j=2}^{n}\frac{(-i)^{j-1}}{j!}k_i^{(j)}\frac{\partial^j}{\partial\tau^j}A_i = \frac{id_{eff}\omega_i}{n_i c}A_p A_s^* e^{-i\Delta kz},$$

in which A_m ($m = p, s,$ and i) is the field amplitude of the pump, signal and idler pulses, respectively, v_{gm} is the group velocity, k_j denotes the jth-order dispersion coefficient, j is calculated up to 4, d_{eff} is the nonlinear coefficient for the parametric amplification, and n_m is the refractive index of each pulse evaluated from the Sellmeier equations. The equations are solved through split-step Fourier-transform algorithm, in which the dispersion is calculated in the frequency domain and the amplification is calculated in the time domain with 4th-order Runge-Kutta numerical method. The interacting pulses are treated with slowly varying envelope approximation (SVEA), which is a reasonable approximation in the investigation because all the involved pulses are stretched to pulse durations longer than 50 fs. Since the input pulses contain spectral bandwidth up to several hundred nanometers, the 3rd-order and 4th-order dispersions are included. However, higher order dispersions show very little influence to the results, therefore neglected in the simulation. Since one-dimensional (1D) numerical model is valid to reveal the spectral-temporal properties in the parametric process, and the spatial distribution of the beams is beyond the scope of this paper, we perform a simple 1D simulation in the following investigation.

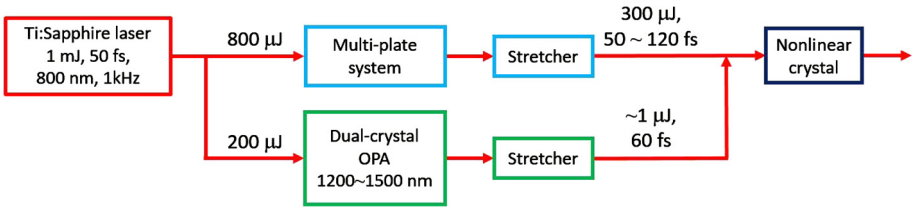

Fig. 1. Schematic of a dual-chirped optical parametric amplifier pumped by a broadband laser pulse.

The interacting pulses are stretched with linear temporal chirp (the time dependence of its instantaneous frequency, with the unit of Hz/fs). However, the dispersions of the pulses are calculated in the frequency domain, therefore the temporal chirp is transformed to the group delay dispersion (GDD) and added to the pulses in the frequency domain. Detailed illustration of the relationship between GDD and temporal chirp can be found in our previous work [47]. The pump chirp can be introduced using either chirped mirrors (negative chirp) or bulk material (positive chirp). At the same time the seed pulse is also stretched to ~60 fs, with a fixed GDD of −180 fs^2. The temporal and frequency pulse shaping can be easily achieved by chirped mirrors or DAZZLER.

During the simulation, we employ the energy-bandwidth product (EBP) to compare the performances of different systems. The pulse EBP is the ratio of its energy to the TL duration, which represents the highest achievable peak power of the pulse. As widely known, there is a tradeoff between the energy conversion efficiency and the gain bandwidth during the parametric amplification, therefore we employ the EBP in order to determine the highest achievable power of the output pulses. A piece of β-barium borate (BBO) crystal is employed as the nonlinear crystal. The applied BBO crystal is cut at 19.9°, which is the phase-matching angle for 1400-nm signal components. The BBO thicknesses are selected in such a way that the EBPs of the output pulses are optimal.

3. Gain mechanism in DC-OPA

Before simulating the parametric amplification, it is necessary to analyze the gain mechanism of OPA system. The gain properties of OPA are built on the amplification of initial seed and idler pulses through the three-wave interaction. For this reason, the initial bandwidth of seed or idler pulse determines the upper limit of achievable bandwidth after the OPA process. The initial bandwidth is defined as the bandwidth obtained in an infinitely thin nonlinear crystal through OPA process. Regarding to an idler pulse, it is produced as soon as the pump and seed pulses are injected into the nonlinear crystal, via difference frequency generation (DFG) between the pump and seed pulses. If the crystal thickness is infinitely close to 0, the initially generated idler bandwidth is thus not affected by the phase-matching condition but mainly determined by the present pump and seed wavelengths.

We then turn to DC-OPA, as previously studied in [37], the dual-chirped geometry allows us to manipulate the initial pump and seed chirps individually. Compared to conventional OPCPA, DC-OPA scheme has more degrees of freedom because the pump chirp is variable as well as the seed chirp. In this case, the system performance is largely dependent on the instantaneous wavelengths of the input pump and seed pulses.

We first show how the pump and seed bandwidths and their chirp combinations affect the initial idler bandwidth. In DC-OPA, the instantaneous frequency of the interacting pulses can be expressed as follows:

$$\omega_p(t) = \omega_{p0} + C_p t,$$

$$\omega_s(t) = \omega_{s0} + C_s t,$$

$$\omega_i(t) = \omega_p(t) - \omega_s(t) = \omega_{i0} + C_i t,$$

in which $\omega_m(t)$ ($m = p$, s, and i) is the time-dependent angular frequency of the pump, signal, and idler pulses, respectively, ω_{m0} is the central angular frequency and C_m is the temporal chirp of each pulse, $C_i = C_p - C_s$. The calculated results are plotted in Fig. 2. Pump pulses with TL durations of 10 fs (black), 20 fs (blue), 30 fs (red) and 50 fs (yellow) are included. The GDDS introduced to the pump pulses are ±90 fs^2, ±165 fs^2, ±215 fs^2, and 0 fs^2, respectively, and all the pump pulses are stretched to the duration of 50 fs. The seed GDD is fixed at −180 fs^2, and the seed pulse is stretched to the duration of 60 fs. Since the gain mechanism of DC-OPA system is independent on the pump-seed duration ratio, we investigate a slightly longer seed pulse than the pump pulse as an example.

When the pump and seed pulses are chirped with the same sign, C_p and C_s are both negative, the instantaneous wavelengths of pump and idler are shown in Fig. 2(a) and (c), respectively. To stretch different pulses to the same duration, the temporal chirp of a broadband pulse is larger than that of a narrowband pulse (absolute value). When the TL duration of the pump is longer than 20 fs, the seed bandwidth is broader than the pump, $|C_s| > |C_p|$. Consequently, the idler pulses are generated with positive chirps ($C_i > 0$, blue, red, and yellow lines in Fig. 2(c)). As TL duration of the pump reaches 10 fs, the pump bandwidth exceeds the seed bandwidth, $|C_p| > |C_s|$, the idler is therefore generated with a negative chirp ($C_i < 0$, black line in Fig. 2(c)). Note that the TL-10-fs pump has a much larger bandwidth than the signal, thus its wavelength slope is much steeper than the seed. As a result, the slope of the black line in Fig. 2(c) is even larger than the yellow line.

When the pump and seed pulses are chirped with opposite signs, $C_p > 0$ and $C_s < 0$, the instantaneous wavelengths are shown in Fig. 2(b) and (d), respectively. As observed in Fig. 2(b), the time-dependent wavelengths of the pump pulses are exactly opposite to the ones in Fig. 2(a), which are opposite to the seed wavelength. In this case, the idler pulses are always generated with a positive initial chirp, $C_i = C_p - C_s = |C_p| + |C_s| > 0$. After stretching different pump pulses to the same duration, the pump pulse with a larger bandwidth contains larger chirp compared to a narrow bandwidth, thus we can plot the instantaneous wavelengths of the idler as in Fig. 2(d), in which the idler chirp from TL-10-fs pump system is the largest among the 4 systems. It is easily deduced that C_i is larger when C_p and C_s have opposite signs, hence the largest initial idler chirp is achieved when the pump and seed pulses are oppositely chirped.

The idler pulse is produced in a time window where the input pump and seed pulses are temporally overlapped. In the above conditions, the stretched pump durations (50 fs) are shorter than the seed (60 fs), thus the durations of the idler pulses in all conditions are close to the input pump pulses. As shown in $\omega_i(t) = \omega_{i0} + C_i t$, when the temporal property of the initially generated idler pulse is fixed, the main factor that determines the idler bandwidth is the pulse chirp C_i. Based on the above analysis, the

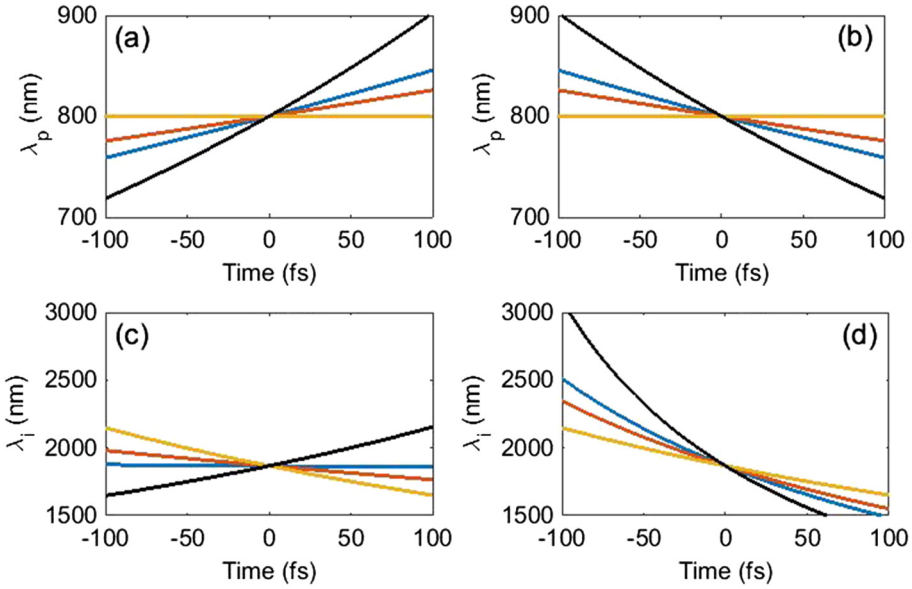

Fig. 2. (a), (b) Time-dependent wavelengths of the pump pulses. (c), (d) Time-dependent wavelengths of the idler pulses. The initial pump chirps in (a) and (c) are negative, the initial pump chirps in (b) and (d) are positive. The black, blue, red, and yellow lines represent pump pulses with TL durations of 10 fs, 20 fs, 30 fs, and 50 fs, respectively. (For interpretation of the references to color in this figure legend, the reader is referred to the web version of this article.)

largest bandwidth of the initially generated idler pulse is obtained with oppositely chirped pump and seed pulses.

In Fig. 3, the phase-matching efficiency with respect to the pump chirp and the idler wavelength is depicted. The seed pulse is still chirped to ~60 fs with a GDD of −180 fs^2 in this condition. The phase-matching efficiency is expressed as $sinc^2(\Delta kL/2)$, where $\Delta k = k_p - k_s - k_i$ is the frequency-dependent phase mismatch and L is the nonlinear crystal thickness. The crystal thickness L is fixed at 2 mm here for simplicity. The white dotted lines in Fig. 3 define the initially generated idler wavelength range within the temporal window of $-50\ fs \leq t \leq 50\ fs$. The GDDs of positively chirped pump pulses with TL durations of 10 fs, 20 fs, 30 fs, and 50 fs are indicated as the black, blue, red, and purple lines, respectively. The pump pulse durations after stretching are all ~50 fs, and the length of each line represent the initially generated idler bandwidth in each condition.

As observed in the bottom half of Fig. 3, high efficiency phase-matching is achieved for the idler components spanning from 1600 nm to 1900 nm by introducing negative chirps for both pump and seed pulses. For the pump pulse with a GDD of −40 fs^2, the phase-matching bandwidth reaches the maximum. This is a linear fit to the aforementioned chirp-compensation scheme as reported in [43,46,48]. However, as depicted by the white lines, the spectrum of the initially generated idler only starts from >1700 nm. For this reason, we have no wavelength components <1700 nm amplified, though this part is still phase matched, and consequently, a narrowed idler bandwidth is obtained after the parametric process. It is observed that the TL-10-fs pump case (GDD = −90 fs^2) has the largest idler bandwidth, and the TL-20-fs (GDD = −165 fs^2) and TL-30-fs (GDD = −215 fs^2) pump cases have similar GDDs to the seed, making the bandwidth of the initially generated idler pulse close to 0. It can be therefore predicted that, when the pump pulse is negatively chirped, the DC-OPA pumped by a TL-10-fs pulse produces idler pulse with the largest bandwidth.

In the top half of Fig. 3 where the pump and seed pulses are oppositely chirped, high efficiency phase-matching bandwidth is slightly narrower than the bottom half while the moderate phase-matched bandwidth is comparatively broader. It is noteworthy that phase-matching is an accumulated effect during the parametric amplification process. Even though the phase-matching bandwidth is narrower, as long as the crystal thickness is appropriate, the wavelength components with moderate phase-matching efficiency still cover a broad bandwidth.

It is also noticed that the pump GDD is of minor influence on the phase-matching efficiency. For different positive pump GDDs, the phase-matching bandwidths are similar, which makes the initial bandwidth defined by the white dotted lines the decisive factor for the idler output bandwidth. The 4 cases are indicated by the solid lines in Fig. 3. The pump pulse with a TL duration of 50 fs needs no further stretching in this condition and the pump GDD is 0. For pump pulses with <50-fs TL duration, as the pump bandwidth increases, the required GDD decreases and the corresponding idler bandwidth becomes broader. Therefore the DC-OPA system pumped by a TL-10-fs pulse is capable of producing the largest idler bandwidth even with a narrower phase-matching bandwidth.

Moreover, it is also found in Fig. 3 that the potentially largest idler bandwidth is actually achieved when the pump GDD is 40 fs^2. In order to apply this particular pump GDD in the proposed scheme while maintain high conversion efficiency, the pump bandwidth should be broad enough to support a TL duration of ~4.5 fs to ensure that the stretched pump duration is 50 fs. With state-of-the-art techniques, near millijoule pulses with even larger bandwidth is readily available [50]. The idler bandwidth and gain efficiency can be further improved simultaneously when the pump pulse with broader bandwidth is employed.

4. Simulation of broadband pumped DC-OPA

In order to further investigate the DC-OPA pumped by broadband laser pulse, the parametric processes in various pump bandwidths and pump-seed chirp combinations are compared. Firstly, we study the condition in which both the pump and seed pulses are negatively chirped, the results are presented in Fig. 4. Fig. 4 (a) and (b) shows the signal bandwidth and EBP variations with respect to the stretched pump duration, and Fig. 4(c) and (d) shows the idler bandwidth and EBP variations, respectively. The black, blue, red, and yellow dots represent pump TL durations of 10 fs, 20 fs, 30 fs, and 50 fs, respectively. Since the signal/idler output

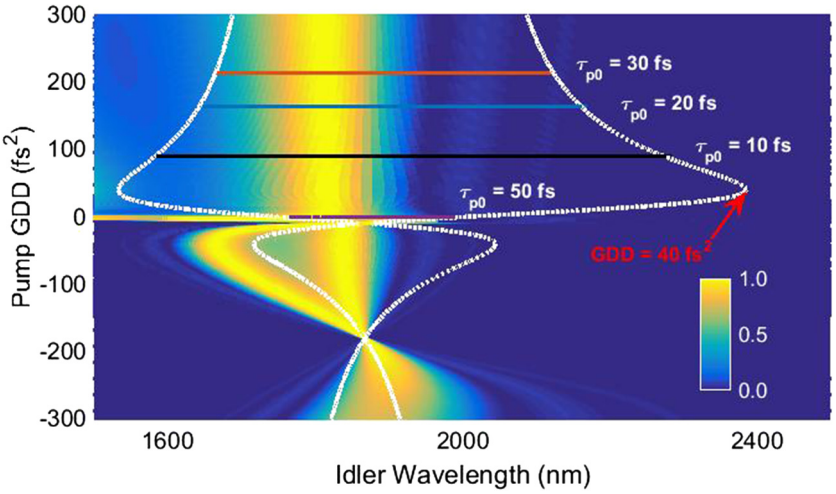

Fig. 3. Phase-matching efficiency at different idler wavelengths and pump GDDs. The white dotted lines represent the idler bandwidth within the temporal range of $-50\ \text{fs} \le t \le 50\ \text{fs}$. The black, blue, red, and purple lines indicate the pump GDDs when the TL durations are 10 fs, 20 fs, 30 fs, and 50 fs respectively. All pump pulses are stretched to 50 fs with their corresponding GDDs. (For interpretation of the references to color in this figure legend, the reader is referred to the web version of this article.)

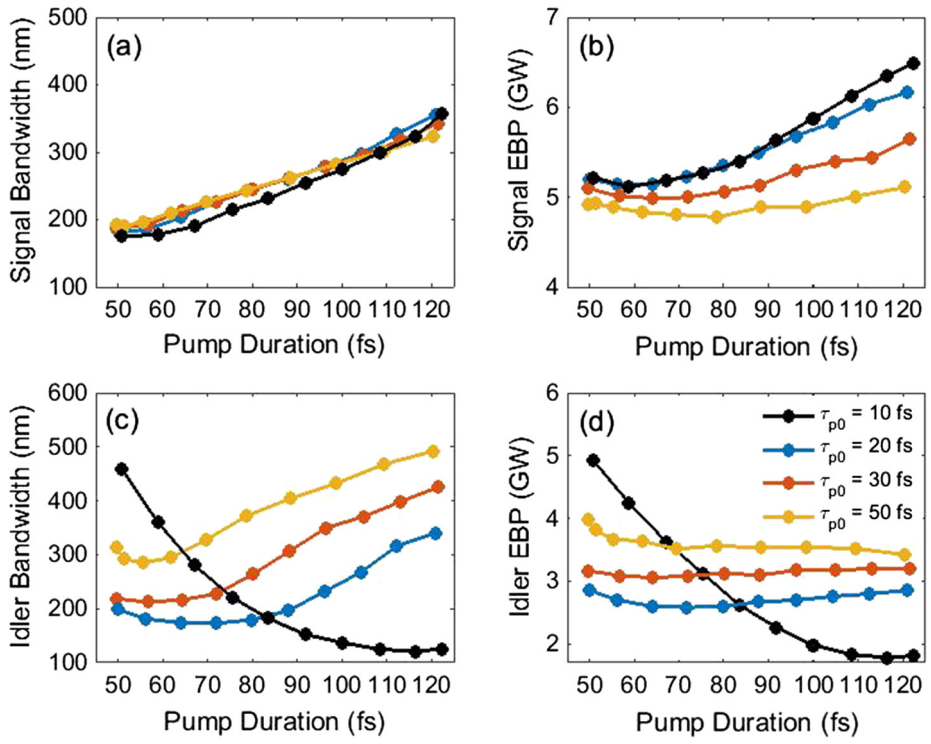

Fig. 4. (a) Signal bandwidth, (b) signal EBP, (c) idler bandwidth, and (d) idler EBP variations with respect to the duration of the stretched pump pulses. Both the pump and seed pulses are negatively chirped.

spectra are not perfectly Gaussian-shaped, we employ the full width at $1/e^2$ maximum (FW1/e^2 M) bandwidth instead of FWHM bandwidth to compare the spectra more accurately [53]. When the pump TL duration is larger than 20 fs, it is shown that the signal bandwidth is barely affected while the idler bandwidth becomes narrower as the TL duration of the pump shortens. In Fig. 4 (b) and (d), the signal EBP increases with the pump bandwidth while the idler EBP decreases. The signal bandwidth and EBP follow the same trend in the 10-fs-pump case, however, the idler shows an irregular trend. Both the bandwidth and EBP of the idler reach the peak when the pump is stretched to 50 fs. As the pump pulse is further stretched, unlike other cases, the idler bandwidth and EBP decreases.

For a fixed pump bandwidth, by stretching the pump pulse to a longer duration with larger GDD, the signal spectrum shows a trend of getting broadened. This is because the pump duration is kept longer than the seed duration during the amplification process, which significantly reduces the gain narrowing effect. In addition, the advantage of signal EBP from a broadband pumped system becomes larger with longer stretched pump duration. Since the signal bandwidth is not dependent on the pump bandwidth in Fig. 4(a), the advantage of EBP indicates an enhancement of the energy conversion efficiency. When the pump pulse is stretched to 120 fs, the signal EBP in the broadband pump system reaches 6.5 GW, which is 27.5% larger than 5.1 GW in the narrowband pump system. The corresponding conversion efficiencies are

20.5% (τ_{p0} = 10 fs) and 18.3% (τ_{p0} = 50 fs), respectively. Despite the obvious improvement of the signal efficiency, a larger pump bandwidth does not favor the idler pulse. The idler bandwidth and EBP are both degraded in the broadband pump system, and even though the idler bandwidth increases with larger GDD, the EBP shows no improvement.

In order to comprehend the unusual trend of the black curves in Fig. 4(c) and (d), we have simulated the conditions where the TL duration of the pump pulses are 12 fs, 15 fs, and 18 fs, respectively. The results are plotted in Fig. 5, in comparison to the TL-10-fs and TL-20-fs pumped cases. It is observed that the trends of the idler bandwidth and EBP are non-monotonic, and they all experience a decrease followed by an increase as the stretched pump duration raises. This is resulted from the temporal chirps of the initial pump and seed pulses.

When the temporal chirp of the seed is larger than that of the pump, the idler is generated with an initial positive chirp. As the stretched pump duration increases, the pump chirp increases while the idler chirp decreases. According to the analysis in Section 3, a smaller initial idler chirp leads to a narrower bandwidth, which explains the decrease in the trends. The minimal points of the curves indicate the condition where the temporal chirps of the pump and seed pulses are equal. The idler pulse is thus produced with minimized chirp in these scenarios, resulting in the least output bandwidth and EBP. As the pump pulse is further stretched, the temporal chirp of the pump pulse exceeds that of the seed, and the idler pulse is produced with an initial negative chirp. Thereafter, further stretching the pump pulse leads to a larger chirp of the idler pulse, and the output idler bandwidth and EBP increase correspondingly.

For pump pulses with different TL durations, the spectral bandwidth is different. At the minimal point of each curve, the temporal chirp of all the pump pulses are the same. In this scenario, with a larger spectral bandwidth (shorter TL duration), the stretched pulse duration would be longer. Consequently, the pump duration at each minimal point reveals a clear shift as the TL pump duration changes.

Experimentally speaking, since the bandwidth broadening approaches such as multi-plate scheme or gas-filled hollow fiber usually introduce positive temporal chirp to the pulse, it is more practical that the pump pulse is stretched with a positive GDD in the proposed scheme. On the other hand, using positively chirped pump and negatively chirped seed pulses, the obtained idler pulse contains a positive chirp, which can be simply compensated by prisms or chirped mirrors. Therefore, next we investigate the system with positively chirped pump and negatively chirped seed, and the results are depicted in Fig. 6. Similar to Fig. 4(a), the broadband pump is not helpful for the signal bandwidth in Fig. 6(a), and on the contrary to Fig. 4(b), the signal EBP in Fig. 6(b) is decreased with a larger pump bandwidth. Nevertheless, the broadband pump is evidently beneficial to the idler pulse when the pump and seed have opposite chirps. Fig. 6(c) and (d) depicts that a larger pump bandwidth can increase both the idler bandwidth and EBP. When the stretched pump duration is 50 fs, the obtained idler spectra cover the bandwidths of 858 nm and 314 nm from the broadband and narrowband pump systems, respectively. Meanwhile, the idler EBPs are 6.9 GW and 4.0 GW, respectively. The 72.6% EBP improvement is mainly originated from the broader output bandwidth and thereby shorter TL duration.

According to the above results, the most intriguing improvement occurs for the idler when the pump and seed pulses are oppositely chirped. Next, we focus on the spectral-temporal properties of different systems where the pump and seed chirps are of opposite signs, and the results are presented in Fig. 7. Fig. 7(a) plots the input (dashed line) and output (solid line) spectra of the signal. Fig. 7(b) shows the idler spectra from systems pumped by pump pulses with TL durations of 10 fs (black line), 20 fs (blue line), 30 fs (red[1] line), and 50 fs (yellow line), respectively. The TL pulse durations here are used for indicating the bandwidth of the pumps, all the pump pulses are actually chirped and stretched to the duration of 50 fs. The GDDs introduced to the pulses are 90 fs^2, 165 fs^2, 215 fs^2, and 0 fs^2, respectively. The stretched pump duration is fixed to ensure that the conversion efficiencies in all cases are similar. This way, a broader idler bandwidth would directly lead to a better system performance. The employed BBO thickness is 2.5 mm in all systems.

In addition, the idler spectrum from an unchirped OPA system (black dashed line) is plotted in Fig. 7(b). The TL pump duration in the unchirped OPA is 10 fs. Note that the unchirped case is only investigated here to verify the bandwidth broadening effect of the dual-chirped geometry. TL pulses have higher peak intensities than the chirped pulses, the available pump energy is therefore limited by the damage threshold of the nonlinear crystal. Practically speaking, using chirped pump pulses allows us to employ higher pulse energy in OPA system, thus achieving a better performance. Besides, with current bandwidth broadening techniques, broadband pump pulses are produced with temporal chirps, and the recompression requires well-arranged dispersion management, which adds complexity to the system.

As observed in Fig. 6(a), the output signal bandwidth from different systems are similar when the stretched pump duration is 50 fs, therefore only one signal spectrum is plotted in Fig. 7(a). It is observed that the signal experiences gain narrowing during the amplification, resulting in a bandwidth of ~100 nm narrower than the input seed. However, owing to the oppositely chirped pump and seed, idler spectrum with much larger bandwidth than signal is obtained. On one hand, the idler bandwidth broadens with the pump bandwidth, the idler bandwidth in broadband pumped system nearly triples compared to the narrowband pumped system. On the other hand, the idler from DC-OPA (black solid line in Fig. 7(b)) has a much broader spectrum than the unchirped OPA (black dashed line in Fig. 7(b)), which indicates that the dual-chirped geometry is valid in further improving the idler bandwidth.

The idler TL durations corresponding to different spectra are depicted in Fig. 7(c). The TL duration of the idler pulse generated in 50-fs pump system is 18.5 fs, nearly 3 optical cycles for 1867-nm pulse. As the pump bandwidth increases, the idler TL duration decreases. In the broadband pumped system, the idler bandwidth is nearly tripled, leading to a significantly shortened TL duration of 8.4 fs, corresponding to ~1.3 optical cycles. The conversion efficiencies for uncompressed idler pulses are 19.1% (TL-10-fs pump), 21.8% (TL-20-fs pump), 22.8% (TL-30-fs pump), and 24.4% (TL-50-fs pump), respectively. Although the conversion efficiency is slightly sacrificed, the much shorter TL duration in broadband pump system compensates the energy loss and still ensures a markedly higher EBP.

Furthermore, the proposed scheme is not limited to 1400-nm signal and 1867-nm idler pulses. After changing the initial pump-seed delay and BBO crystal angle, the system also works well in amplifying other non-degenerate central wavelengths. As shown in Fig. 8(a), the idler spectra obtained from a broadband pump OPA system varies from 1700 nm to 2050 nm, with over 600-nm FW1/e^2 M bandwidth at all central wavelengths. Since there is a strong absorption for >2200-nm components in BBO crystal, we have included the absorption ratio during the simulation, which leads to the intensity drop of the spectra in Fig. 8(a). Fig. 8(b) plots the conversion efficiencies and TL durations of idler pulses at dif-

[1] For interpretation of color in 'Fig. 7', the reader is referred to the web version of this article.

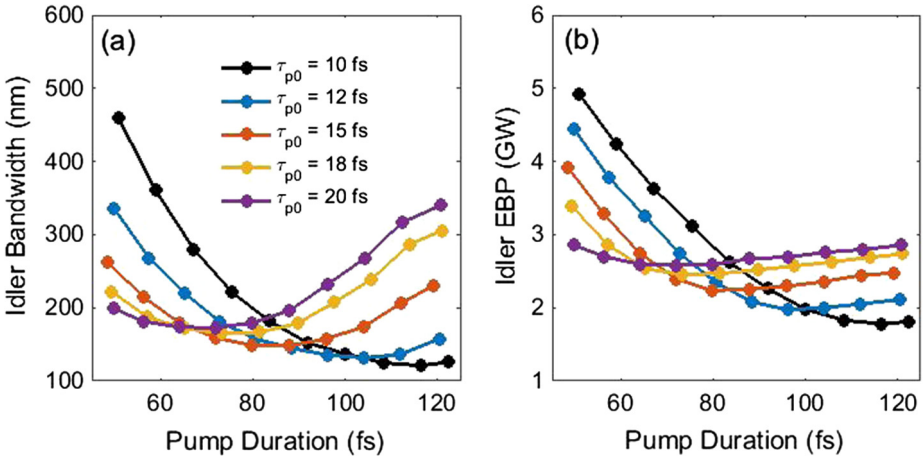

Fig. 5. Idler bandwidth (a) and EBP (b) variations with respect to the duration of stretched pump pulses. The TL durations of the pump pulses are 10 fs, 12 fs, 15 fs, 18 fs, and 20 fs, respectively.

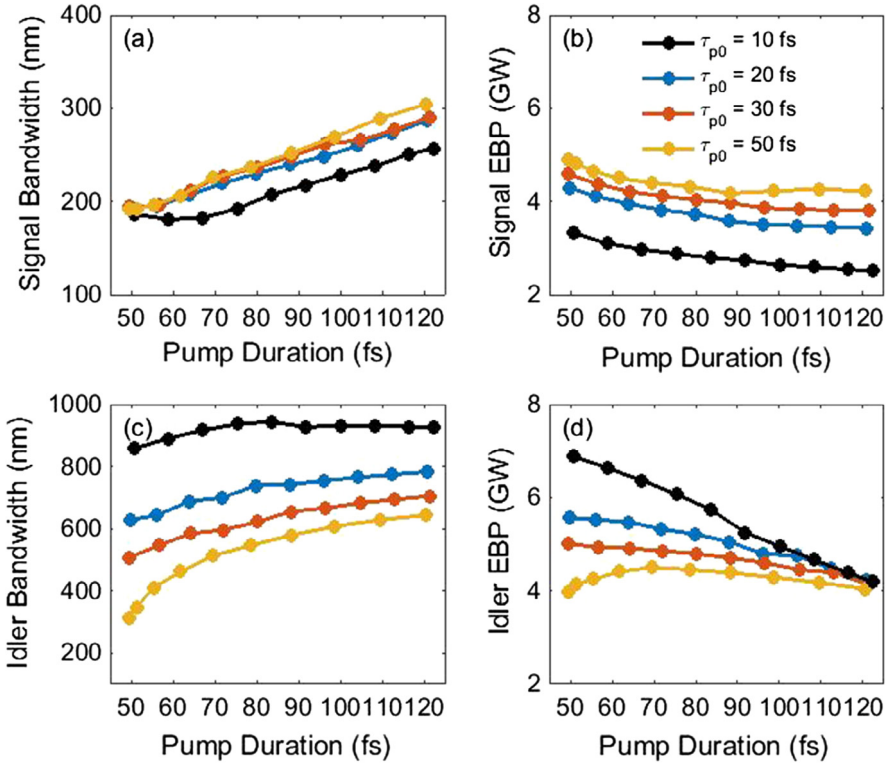

Fig. 6. (a) Signal bandwidth, (b) signal EBP, (c) idler bandwidth, and (d) idler EBP variations with respect to the duration of the stretched pump pulses. The pump pulses are positively chirped and the seed pulses are negatively chirped.

ferent central wavelengths, all pulses can be compressed to a TL duration of <9 fs, corresponding to less than 1.5 optical cycles, with a conversion efficiency larger than 14%, which reveals the high tunability of the broadband pumped OPA in the non-degenerate spectral range.

Last but not least, it is worth emphasizing that we selected the pump and seed energy in the above simulations to reveal the basic principle of the proposed scheme. In previous researches regarding DC-OPA, one of its biggest advantages is the energy scalability, which also exists in our proposed scheme. The highest peak intensity of the pump pulse in our investigation is only 15.3 GW/cm^2 (300 μJ, 50 fs, 5 mm), which is much lower than the damage threshold of BBO crystal. Therefore, it is reasonable to deduce that higher pump energy can be employed in the proposed scheme. Besides, in order to produce few-cycle pulses with higher energy, the broadband pump and seed pulses can be further stretched to contain more energy while keep the peak intensity under the damage threshold of nonlinear crystal. As the pump pulse energy increases, the high conversion efficiency ensures that the broadband pump DC-OPA is still capable of generating hundred-microjoule or even multi-millijoule few-cycle pulses in the infrared region. On the other hand, with the currently available pump

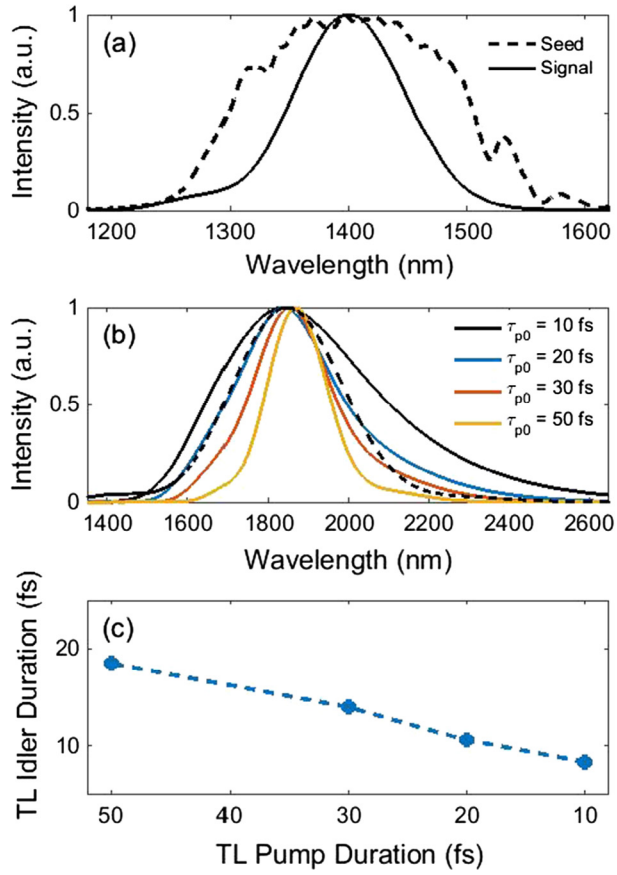

Fig. 7. (a) Input (dashed line) and output (solid line) spectra of the signal. (b) Output spectra of idler pulses from systems with different pump bandwidths. Idler spectrum from an unchirped OPA (black dashed line) is plotted for comparison. (c) The TL duration of output idler pulse with respect to the pump TL duration.

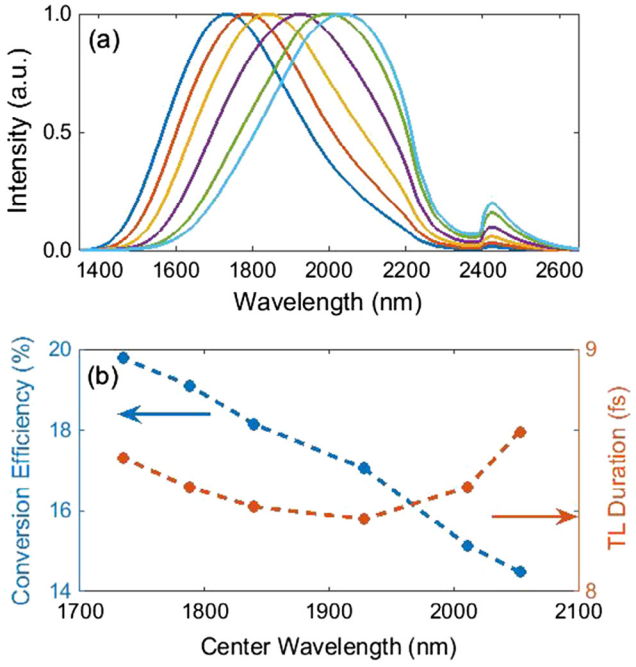

Fig. 8. (a) Idler spectra centered at different wavelengths. (b) Conversion efficiency and TL duration variations of the idler pulses at different center wavelengths.

energy, the uncompressed idler energy is over 50 μJ, which makes it a suitable source for seeding a mid-IR OPCPA with higher pulse energy.

5. Conclusions

In conclusion, we have proposed and investigated the DC-OPA scheme pumped by a broadband laser pulse. By broadening the spectral bandwidth of the pump and chirping both pump and seed pulses before entering the nonlinear crystal, the system performance is remarkably enhanced. The mechanism for the improvement of system performance is analyzed and discussed in detail. The output idler bandwidth is affected by both the initial wavelength components within its temporal profile and the phase-matching efficiency during the amplification. Based on thorough investigation on the combined influence of these two factors, the advantages of broadband pump and oppositely dual-chirped geometry are confirmed.

The broadband pumped DC-OPA scheme is simulated in various conditions and the results are compared. When the pump and seed chirps are of opposite signs, the idler benefits most efficiently from both the broader pump bandwidth and the dual-chirped geometry. The idler bandwidth is nearly tripled compared to that of the narrowband pump system, which supports a TL duration of 8.4 fs (~1.3 optical cycles at 1867 nm), meanwhile the pulse EBP is increased by over 70%. Broadband tunable idler pulses are obtained by slightly altering the pump-seed delay and crystal angle, sub-1.5-cycle TL duration and over 14% conversion efficiency can be achieved simultaneously. The few-cycle tunable pulses from the proposed scheme makes it also a potential candidate working as the driving laser source for scaling the XUV photon energy in high-order harmonic generation (HHG) [54,55]. The maximum photon energy is improved by 45% if the central wavelength of driving laser is tuned from 1700 nm to 2100 nm. Moreover, it is found that the idler bandwidth and EBP can be further improved with a broader pump bandwidth.

The proposed scheme shows great potential in generating energy scalable few-cycle pulses and seeding more energetic OPCPA systems. We believe that the broadband pumped DC-OPA system will contribute to the development of not only ultrafast coherent X-ray generation but also strong-field physics researches.

Funding

This work is supported by grant (No. 11574101, 11234004, 61275126) from National Natural Science Foundation of China.

References

[1] T. Brabec, F. Krausz, Rev. Mod. Phys. 72 (2) (2000) 545–591.
[2] F. Krausz, M. Ivanov, Rev. Mod. Phys. 81 (1) (2009) 163–234.
[3] E. Goulielmakis, M. Schultze, M. Hofstetter, V.S. Yakovlev, J. Gagnon, M. Uiberacker, A.L. Aquila, E.M. Gullikson, D.T. Attwood, R. Kienberger, F. Krausz, U. Kleineberg, Science 320 (2008) 1614–1617.
[4] C. Zhai, L. He, P. Lan, X. Zhu, Y. Li, F. Wang, W. Shi, Q. Zhang, P. Lu, Sci. Rep. 6 (2016) 23236.
[5] M. Qin, X. Zhu, Opt. Laser Technol. 87 (2017) 79–86.
[6] P. Lan, M. Ruhmann, L. He, C. Zhai, F. Wang, X. Zhu, Q. Zhang, Y. Zhou, M. Li, M. Lein, P. Lu, Phys. Rev. Lett. 119 (2017) 033201.
[7] C. Zhai, X. Zhu, P. Lan, F. Wang, L. He, W. Shi, Y. Li, M. Li, Q. Zhang, P. Lu, Phys. Rev. A 95 (2017) 033420.
[8] Z. Wang, M. Li, Y. Zhou, P. Lan, P. Lu, Sci. Rep. 7 (2017) 42585.
[9] L. Li, Z. Wang, F. Li, H. Long, Opt. Quant. Electron. 49 (2017) 73.
[10] X. Ma, M. Li, Y. Zhou, P. Lu, Opt. Quant. Electron. 49 (2017) 170.
[11] S. Ke, B. Wang, C. Qin, H. Long, K. Wang, P. Lu, J. Lightw. Technol. 34 (22) (2016) 5258–5262.
[12] G.F. Albrecht, J.M. Eggleston, J.J. Ewing, Opt. Commun. 52 (6) (1985) 401–404.
[13] P.F. Moulton, J. Opt. Soc. Am. B 3 (1) (1986) 125–133.
[14] D. Strickland, G. Mourou, Compression of amplified chirped optical pulses, Opt. Commun. 56 (3) (1985) 219–221.

[15] G. Cerullo, S. De Silvestri, Rev. Sci. Instrum. 74 (1) (2003) 1–18.
[16] D. Brida, C. Manzoni, G. Cirmi, M. Marangoni, S. Bonora, P. Villoresi, S. De Silvestri, G. Cerullo, J. Opt. 12 (1) (2010) 013001.
[17] S. Witte, K.S.E. Eikema, IEEE J. Sel. Top. Quantum Electron. 18 (1) (2012) 296–305.
[18] J. Biegert, P.K. Bates, O. Chalus, IEEE J. Sel. Top. Quantum Electron. 18 (1) (2012) 531–540.
[19] D. Brida, G. Cirmi, C. Manzoni, S. Bonora, P. Villoresi, S. De Silvestri, G. Cerullo, Opt. Lett. 33 (7) (2008) 741–743.
[20] A.M. Siddiqui, G. Cirmi, D. Brida, F.X. Kärtner, G. Cerullo, Opt. Lett. 34 (22) (2009) 3592–3594.
[21] N. Ishii, K. Kaneshima, K. Kitano, T. Kanai, S. Watanabe, J. Itatani, Opt. Lett. 37 (20) (2012) 4182–4184.
[22] R. Dabu, Opt. Express 18 (11) (2010) 11689–11699.
[23] O. Isaienko, E. Borguet, P. Vöhringer, Opt. Lett. 35 (22) (2010) 3832–3834.
[24] C. Schmidt, J. Bühler, A.-C. Heinrich, A. Leitenstorfer, D. Brida, J. Opt. 17 (2015) 094003.
[25] D. Brida, S. Bonora, C. Manzoni, M. Marangoni, P. Villoresi, S. De Silvestri, G. Cerullo, Opt. Express 17 (15) (2009) 12510–12515.
[26] M. Liebel, C. Schnedermann, P. Kukura, Opt. Lett. 39 (14) (2014) 4112–4115.
[27] D. Herrmann, L. Veisz, R. Tautz, F. Tavella, K. Schmid, V. Pervak, F. Krausz, Opt. Lett. 34 (16) (2009) 2459–2461.
[28] C. Zhang, P. Wei, Y. Huang, Y. Leng, Y. Zheng, Z. Zeng, R. Li, Z. Xu, Opt. Lett. 34 (18) (2009) 2730–2732.
[29] T. Kobayashi, A. Shirakawa, Appl. Phys. B 70 (2000) S239–S246.
[30] Y. Deng, A. Schwarz, H. Fattahi, M. Ueffing, X. Gu, M. Ossiander, T. Metzger, V. Pervak, H. Ishizuki, T. Taira, T. Kobayashi, G. Marcus, F. Krausz, R. Kienberger, N. Karpowicz, Opt. Lett. 37 (23) (2012) 4973–4975.
[31] T. Fuji, N. Ishii, C.Y. Teisset, X. Gu, Th. Metzger, A. Baltuška, N. Forget, D. Kaplan, A. Galvanauskas, F. Krausz, Opt. Lett. 31 (8) (2006) 1103–1105.
[32] K.-H. Hong, S.-W. Huang, J. Moses, X. Fu, C.-J. Lai, G. Cirmi, A. Sell, E. Granados, P. Keathley, F.X. Kärtner, Opt. Express 19 (16) (2011) 15538–15548.
[33] C. Li, D. Wang, L. Song, J. Liu, P. Liu, C. Xu, Y. Leng, R. Li, Z. Xu, Opt. Express 19 (7) (2011) 6783–6789.
[34] B.E. Schmidt, A.D. Shiner, P. Lassonde, J.-C. Kieffer, P.B. Corkum, D.M. Villeneuve, F. Légaré, Opt. Express 19 (7) (2011) 6858–6864.
[35] B.E. Schmidt, N. Thiré, M. Boivin, A. Laramée, F. Poitras, G. Lebrun, T. Ozaki, H. Ibrahim, F. Légaré, Nat. Commu. 5 (2014) 3643.
[36] P. Lassonde, N. Thire, L. Arissian, G. Ernotte, F. Poitras, T. Ozaki, A. Laramee, M. Boivin, H. Ibrahim, F. Légaré, B.E. Schmidt, IEEE J. Sel. Top. Quantum Electron. 21 (5) (2015) 8700410.
[37] Q. Zhang, E.J. Takahashi, O.D. Mücke, P. Lu, K. Midorikawa, Opt. Express 19 (8) (2011) 7190–7212.
[38] Y. Fu, E.J. Takahashi, K. Midorikawa, Opt. Lett. 40 (21) (2015) 5082–5085.
[39] Y. Fu, E.J. Takahashi, Q. Zhang, P. Lu, K. Midorikawa, J. Opt. 17 (2015) 124001.
[40] S. Wandel, M. Lin, Y. Yin, G. Xu, I. Jovanovic, J. Opt. Soc. Am. B 33 (8) (2016) 1580–1587.
[41] N. Ishii, K. Kaneshima, K. Kitano, T. Kanai, S. Watanabe, J. Itatani, Nat. Commun. 5 (2014) 3331.
[42] Q. Zhang, L. He, P. Lan, P. Lu, Opt. Express 22 (11) (2014) 13213–13233.
[43] Y. Tang, I.N. Ross, C. Hernandez-Gomez, G.H.C. New, I. Musgrave, O.V. Chekhlov, P. Matousek, J.L. Collier, Opt. Lett. 33 (20) (2008) 2386–2388.
[44] J. Limpert, C. Aguergaray, S. Montant, I. Manek- Hönninger, S. Petit, D. Descamps, E. Cormier, F. Salin, Opt. Express 13 (19) (2005) 7386–7392.
[45] P. Baum, S. Lochbrunner, E. Riedle, Appl. Phys. B 79 (8) (2004) 1027–1032.
[46] S. Zeng, B. Zhang, Y. Dan, X. Li, N. Sun, Z. Sui, Opt. Commun. 283 (20) (1992) 4054–4058.
[47] Z. Hong, Q. Zhang, P. Lan, P. Lu, Opt. Express 22 (5) (2014) 5544–5557.
[48] Y. Yin, J. Li, X. Ren, Y. Wang, A. Chew, Z. Chang, Opt. Express 24 (22) (2016) 24989–24998.
[49] C. Lu, Y. Tsou, H. Chen, B. Chen, Y. Cheng, S. Yang, M. Chen, C. Hsu, A. Kung, Optica 1 (6) (2014) 400–406.
[50] P. He, Y. Liu, K. Zhao, H. Teng, X. He, P. Huang, H. Huang, S. Zhong, Y. Jiang, S. Fang, X. Hou, Z. Wei, Opt. Lett. 42 (3) (2017) 474–477.
[51] Z. Hong, Q. Zhang, P. Lu, Opt. Express 21 (8) (2013) 9491–9504.
[52] S.A. Rezvani, Q. Zhang, Z. Hong, P. Lu, Opt. Express 24 (10) (2016) 11187–11198.
[53] B. Xu, Y. Coello, V.V. Lozovoy, D.A. Harris, M. Dantus, Opt. Express 14 (22) (2006) 10939–10944.
[54] B. Shan, A. Cavalieri, Z. Chang, Appl. Phys. B 74 (2002) S23–S26.
[55] A.D. Shiner, C. Trallero-Herrero, N. Kajumba, H.-C. Bandulet, D. Comtois, F. Légaré, M. Giguere, J.-C. Kieffer, P.B. Corkum, D.M. Villeneuve, Phys. Rev. Lett. 103 (2009) 073902.